

AGORA: Adversarial Generation Of Real-time Animatable 3D Gaussian Head Avatars

Ramazan Fazylov
MBZUAI

ramazan.fazylov@mbzuai.ac.ae

Sergey Zagoruyko
Polynome AI

s.zagoruyko@polynome.ai

Aleksandr Parkin
MTS AI

parkin.msu@gmail.com

Stamatis Lefkimmiatis
MTS AI

s.lefkimmiatis@mts.ai

Ivan Laptev
MBZUAI

ivan.laptev@mbzuai.ac.ae

Abstract

The generation of high-fidelity, animatable 3D human avatars remains a core challenge in computer graphics and vision, with applications in VR, telepresence, and entertainment. Existing approaches based on implicit representations like NeRFs suffer from slow rendering and dynamic inconsistencies, while 3D Gaussian Splatting (3DGS) methods are typically limited to static head generation, lacking dynamic control. We bridge this gap by introducing AGORA, a novel framework that extends 3DGS within a generative adversarial network to produce animatable avatars. Our key contribution is a lightweight, FLAME-conditioned deformation branch that predicts per-Gaussian residuals, enabling identity-preserving, fine-grained expression control while allowing real-time inference. Expression fidelity is enforced via a dual-discriminator training scheme leveraging synthetic renderings of the parametric mesh. AGORA generates avatars that are not only visually realistic but also precisely controllable. Quantitatively, we outperform state-of-the-art NeRF-based methods on expression accuracy while rendering at 250+ FPS on a single GPU, and, notably, at ~9 FPS under CPU-only inference – representing, to our knowledge, the first demonstration of practical CPU-only animatable 3DGS avatar synthesis. This work represents a significant step toward practical, high-performance digital humans. Project website: <https://ramazan793.github.io/AGORA/>

1. Introduction

The creation of realistic and controllable digital humans is a significant area of research within computer graphics and computer vision. Demand for high-fidelity avatars is rapidly increasing across applications ranging from immersive VR/AR experiences and telepresence to the entertain-

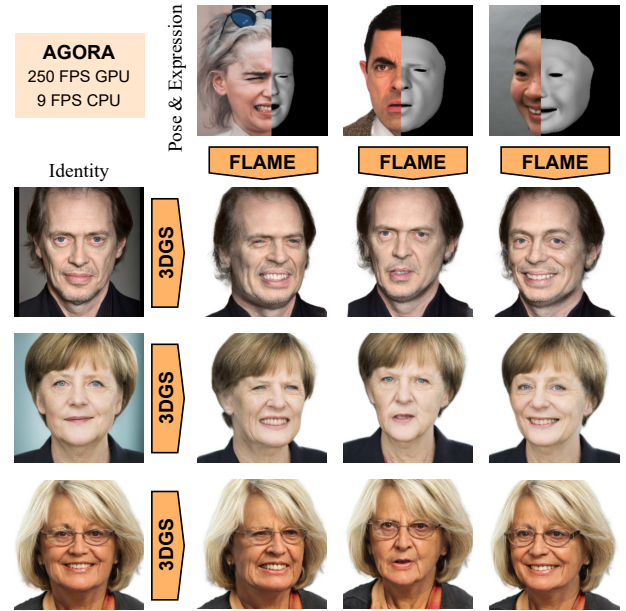


Figure 1. Our method, AGORA, generates animatable 3D avatars. AGORA produces highly photorealistic identity-preserving results and supports dynamic control on pose and face expressions, while allowing real time inference at 250+ FPS on a single GPU.

ment industry. For these applications to be effective, avatars must not only look realistic but also be able to produce accurate expressions. However, generating avatars that are visually convincing, easily animatable, and computationally efficient remains a complex challenge that motivates the exploration of new synthesis and animation techniques.

Recent progress in avatar creation can be broadly categorized into three paradigms. The first, reconstruction-based methods, optimize a 3D representation to fit multi-view [19, 45, 61, 66] or monocular videos [9, 17, 18, 21, 70, 71, 74]. While capable of producing high-fidelity re-

sults for a specific subject, these approaches require lengthy per-subject optimization and often struggle to generalize to novel expressions. A second paradigm leverages large-scale 2D diffusion models via score distillation sampling (SDS) [23, 44, 55, 73] to generate 3D assets from text or a single image. However, these methods often face challenges with view-consistency and achieving the level of detail required for realistic human heads. The most promising direction for generating diverse, high-quality avatars has been 3D-aware Generative Adversarial Networks (3D GANs) [1, 5, 6, 8, 12, 25, 32, 33, 39, 49–51], which learn a distribution of 3D heads from 2D image collections [26, 63]. While some works have extended 3D GANs to dynamic scenarios [2, 11, 24, 53, 54, 62, 64], they typically rely on computationally expensive neural fields. Concurrently, recent advances in static generation have adopted the highly efficient 3D Gaussian Splatting representation [6, 25, 32], but lack animation capabilities. This leaves a critical gap: a method that combines the generative power of 3D GANs with the real-time rendering of 3DGS to create fast, explicit and precisely-animated avatars. Recent concurrent work, GAIA [68], attempts to fill this gap by incorporating expression conditioning to produce animatable avatars. However, this method, while promising, still faces challenges in both inference speed and animation fidelity.

To address this, we introduce a novel framework for generating animatable 3D head avatars that unites the efficiency of 3DGS with the generative power of 3D GANs. Our approach builds upon a static generator, inspired by GGHEAD [32], which produces a canonical set of 3DGS attributes. To enable animation, we introduce our primary contribution: a lightweight, FLAME-conditioned [35] deformation branch. This branch predicts attribute residuals for the canonical Gaussians, efficiently modeling the complex, non-linear motions of facial expressions. This design choice not only disentangles static identity from dynamic articulation but also facilitates real-time animation, as the main generator only needs to be run once per identity. To ensure the generator faithfully adheres to the expression controls, we employ a dual-discrimination scheme that provides adversarial supervision on both the rendered appearance and the underlying geometry. Crucially, we train from static face images only, without multi-view capture or video supervision. The resulting model generates high-fidelity, controllable avatars capable of real-time rendering. Our contributions can be outlined as following:

- A novel architecture for conditional 3D GANs, featuring a lightweight, FLAME-conditioned deformation branch that learns attribute residuals, and a simple spatial identity conditioning of the main branch to help disentangle identity from expression;
- An effective adversarial training strategy using a dual-discriminator on both rendered images and synthetic ge-

ometry cues to enforce expression consistency;

- State-of-the-art results in controllable animation, demonstrating superior expression fidelity and a significant leap in rendering performance (250fps GPU, 9fps CPU) over previous animatable avatar methods.

2. Related Work

Related works can be categorized into static 3D GANs and animatable 3D GANs.

Static 3D head avatars. A significant line of research focuses on training generative adversarial networks on 2D image datasets like FFHQ [26] to produce 3D-consistent outputs. Early works [3, 5, 8, 12, 22, 39, 41, 42, 49, 72] incorporated implicit neural radiance fields (NeRF) [37] into 2D GAN frameworks to enable 3D-consistent generation. To improve rendering speed and view consistency, hybrid NeRF-based representations were introduced [4, 34, 38] and adopted by subsequent methods [6, 39, 41, 50, 51, 59, 65]. Among these, several methods employ a super-resolution network to further accelerate rendering at the cost of some view consistency [6, 39, 41, 59, 65]. In particular, EG3D [6] builds upon the StyleGAN [28] architecture to generate an intermediate triplane representation, which is then rendered into a low-resolution image and further upsampled [60]. While producing high-fidelity results, this reliance on NeRF leads to slow training and inference and introduces 3D inconsistency artifacts due to the super-resolution network. To address this performance bottleneck, subsequent works replaced the NeRF renderer with the highly efficient 3D Gaussian Splatting (3DGS) representation. For instance, GGHEAD [32] generates 3DGS attributes in a UV space mapped to a 3DMM template, while GSGAN [25] directly generates a 3D point cloud in a coarse-to-fine manner. Although these methods achieve real-time rendering, they are fundamentally designed for static head generation.

Dynamic 3D head avatars. Another line of work extends 3D GANs to model facial dynamics [2, 11, 24, 52–54, 62, 64]. Some methods control articulations by conditioning generation on semantic maps [24, 52, 53]; however, such conditioning can yield inconsistent animation in videos. An alternative approach is to condition the generator on parameters of 3D morphable models (3DMM) [35, 36, 43]. Several approaches [2, 62, 64] also predict deformation fields to warp a canonical representation with respect to given 3DMM parameters. One recent work, Next3D [54], incorporates 3DMM more directly: it adapts the EG3D framework by rasterizing neural textures on an articulated FLAME mesh and projecting the head onto orthogonal triplanes. To enforce geometric consistency, it introduces dual discrimination supervising the generator with synthetic renderings of the FLAME geometry. While this enables animation control, expression fidelity can degrade

on complex motions, and dependence on an implicit representation leads to slow inference. Our work addresses this limitation by integrating animation control into a 3DGS-based 3D GAN, achieving both high-fidelity animation and real-time performance. Concurrent work [68] explores a similar direction. However, we show that our methodology yields higher quality avatars and superior rendering speed.

3D head avatars from single image. Orthogonal to the generative task, another goal is to perform animation directly from a single input image [15, 31, 56, 67, 69]. Some recent methods, such as Live3DPortrait [7], focus on generating high-quality static portraits, which, while impressive, do not produce animatable models. Building on this idea, methods like Portrait4D [13, 14] and VOODOO [57, 58] aim to produce fully animatable avatars. These approaches typically operate by leveraging a pre-trained 3D GAN, either by distilling it into a direct image-to-avatar encoder or by training an encoder on a large-scale synthetic dataset generated by the GAN. While these models offer impressive single-shot performance, their quality is fundamentally dependent on the underlying generative model. More recently, GAGAvatar [10] has demonstrated that it is possible to utilize strong semantic features from DiNO [40] to obtain animatable 3D Gaussian representations of a head. However, GAGAvatar’s approach is limited by its reliance on a single dataset [63], making it prone to poor performance on expressions and appearances not represented in the training data. In contrast, our work focuses on enhancing 3D-aware generative models, thereby strengthening GAN-dependent single-shot pipelines. Our approach is complementary to feature-driven methods like GAGAvatar, offering a different pathway to animatable avatars by focusing on improving generative accuracy and real-time performance.

3. Method

In this section we introduce preliminary concepts followed by a concise description of our approach.

3.1. Preliminaries

3D Gaussian Splatting. 3DGS [30] is an explicit 3D representation that models a scene as a collection of 3D Gaussians, enabling high-quality, real-time rendering. Each Gaussian is defined by a position $\mu \in \mathbb{R}^3$, a covariance matrix $\Sigma \in \mathbb{R}^{3 \times 3}$ (parameterized by a scale vector and a rotation quaternion), view-dependent color represented by spherical harmonics (SH) coefficients c , and an opacity α . The color C of a pixel is computed by alpha-blending N Gaussians sorted by depth:

$$C = \sum_{i=1}^N c_i \alpha'_i \prod_{j=1}^{i-1} (1 - \alpha'_j), \quad (1)$$

where α'_i is the opacity of the i -th Gaussian modulated by its 2D projection onto the pixel. This process is differentiable allowing for gradient-based optimization of all parameters.

FLAME 3D Morphable Model. FLAME [35] is a statistical head model that provides a low-dimensional parametric space for shape β , expression ψ , and pose θ . The template T_P is formed by adding linear combinations of shape blendshapes $B_S(\beta)$, expression blendshapes $B_E(\psi)$, and pose-corrective blendshapes $B_P(\theta)$ to a base template \bar{T} :

$$T_P(\beta, \psi, \theta) = \bar{T} + B_S(\beta; \mathcal{S}) + B_E(\psi; \mathcal{E}) + B_P(\theta; \mathcal{P}). \quad (2)$$

After applying linear blend skinning W , we get the articulated model $M(\beta, \psi, \theta) = W(T_P(\beta, \psi, \theta), \mathcal{J}(\beta), \theta, W)$. This formulation allows for fine-grained control over facial identity and articulation. In this work, we primarily leverage the expression parameters ψ and the jaw pose θ to drive the animation of our generated avatars.

3.2. Architecture Overview

The overall architecture of our generative model \mathcal{G} , illustrated in Figure 2(b), builds upon the UV-based GGHEAD framework. Our goal is to produce an animatable 3DGS avatar from a latent code $z \in \mathcal{Z}$, camera parameters π , and FLAME parameters (β, ψ, θ) . Following EG3D [6], a mapping network \mathcal{M} maps the latent code z and camera parameters π to an intermediate latent variable $w \in \mathcal{W}$. The core generator \mathcal{G} then synthesizes a set of UV-space feature maps F_{uv} from w and β , which encode the identity-specific, canonical Gaussian attributes:

$$w = \mathcal{M}(z, \pi), \quad F_{uv} = \mathcal{G}(w, \beta). \quad (3)$$

We obtain the raw Gaussian attributes \mathcal{A}_M by bilinearly sampling F_{uv} at a set of pre-defined UV coordinates x_{uv} :

$$\mathcal{A}_M = \text{GridSample}(F_{uv}, x_{uv}), \quad (4)$$

where $\mathcal{A}_M = \{\mu_{\delta M}, s, q, c, \alpha\}$ includes a position offset $\mu_{\delta M}$ relative to the template mesh M , as well as scale s , rotation q , color c , and opacity α .

The final 3D position of each Gaussian is obtained via *3D lifting*: we bilinearly interpolate a base position from the articulated FLAME mesh $M(\beta, \psi, \theta)$ at x_{uv} and add the predicted offset,

$$\mu = \text{Interpolate}(M(\beta, \psi, \theta), x_{uv}) + \mu_{\delta M}. \quad (5)$$

This design anchors the generated 3DGS to the underlying parametric mesh, providing a structured basis for animation.

3.3. Spatial Shape Conditioning

We condition the main generator \mathcal{G} on the FLAME shape code β to encode shape-specific priors (e.g. smaller cranio-facial proportions for children). We found that naively injecting β into the mapping network \mathcal{M} makes the intermediate latent w predominantly a function of β , which reduces z -driven diversity and leads to mode collapse.

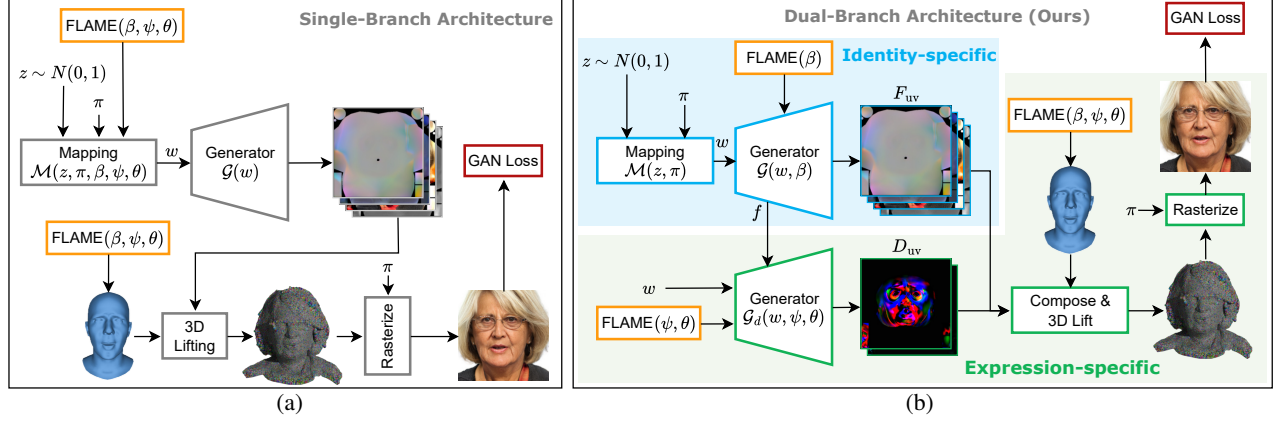


Figure 2. Single- and dual-branch generator designs and expression conditioning. (a) Single-branch GGHEAD-style baseline with no FLAME conditioning; orange box marks conditioning hook used in our ablations: (β, ψ, θ) injected into the mapping network \mathcal{M} . (b) Dual-branch AGORA: an identity path $\mathcal{G}(w, \beta)$ produces canonical 3DGS attributes, while an expression path $\mathcal{G}_d(w, \psi, \theta; f)$ predicts residuals. Residuals are composed with the canonical attributes, 3D lifted onto the articulated FLAME mesh, and rasterized.

Instead, we adopt a softer, spatial conditioning strategy: we derive a UV-aligned map of the *shape-isolated* deformation field and concatenate it to the feature maps within \mathcal{G} . Concretely, with β_{neutral} denoting the canonical neutral shape code, we compute

$$\Delta V_{\text{shape}}(\beta) = M(\beta, \psi_{\text{neutral}}, \theta_{\text{neutral}}) - M(\beta_{\text{neutral}}, \psi_{\text{neutral}}, \theta_{\text{neutral}}). \quad (6)$$

We then bake ΔV_{shape} into a UV-aligned displacement map, apply *per-sample variance normalization* to better match the unit-variance assumption of the StyleGAN-style synthesis network, and concatenate resulting channels with the block features. This spatial, UV-consistent conditioning injects shape biases where they matter geometrically while preserving the stochasticity carried by z .

3.4. Deformation Branch

To refine the coarse 3DMM-based articulation and add high-frequency changes, we introduce a separate, lightweight deformation branch \mathcal{G}_d . This branch takes low-resolution 64×64 feature maps f from the main generator, which encode coarse structural features (e.g., face shape, hair regions) [27], and is conditioned on the FLAME expression ψ and jaw pose θ via style modulation. It produces expression-specific features D_{uv} for the geometric Gaussian attributes:

$$D_{\text{uv}} = \mathcal{G}_d(w, \psi, \theta; f). \quad (7)$$

From these, we obtain residual Gaussian attributes A_D by bilinearly sampling D_{uv} at UV coordinates x_{uv} , where $A_D = \{\Delta\mu, \Delta s, \Delta q\}$. These residuals are then *composed* with the canonical attributes from the main branch to obtain the final Gaussian attributes \mathcal{A} . Specifically, we use post-activation summation for means, quaternion multiplication for rotations, and summation for log-scales.

This design is crucial for two reasons: (1) it prevents identity-expression entanglement, as naively conditioning the main generator \mathcal{G} on expression parameters would cause the model to learn a unique identity for each expression vector; and (2) it enables fast, real-time animation of a fixed identity, since the more computationally expensive identity-specific \mathcal{G} only needs to be run once.

Single vs. dual branch and expression conditioning.

For context, Fig. 2(a) shows the single-branch GGHEAD-style baseline: a single generator with *no* FLAME conditioning. The orange callouts in (a) mark conditioning hook we ablate: injecting (β, ψ, θ) into \mathcal{M} . Our final model follows the dual-branch design in Fig. 2(b). The identity-specific path $\mathcal{G}(w, \beta)$ produces canonical attributes, while the expression-specific branch $\mathcal{G}_d(w, \psi, \theta; f)$ uses w and intermediate features f to predict residuals. We compose these with the canonical attributes, apply 3D lifting (“Compose & 3D Lift” in the figure), and then rasterize.

3.5. Final Gaussian Model

We apply activation functions similar to GGHEAD on the predicted position and scale of the Gaussians. For the position offsets, we use a bounded tanh, which upper-bounds the maximal deviation of Gaussians from the template mesh by γ_{pos} . For the scale parameters, we use a bounded exponential with softplus, which constrains the maximum scale to $e^{-s_{\text{max}}}$ while initializing it at $e^{-s_{\text{init}}}$. Finally, we rasterize the Gaussian model \mathcal{A} with camera parameters π to produce the generated image.

3.6. Enforcing Expression Consistency

Naively training the generator with only an image-based discriminator is insufficient to enforce precise expression control. Following Next3D [54], we adopt a dual-discrimination scheme that conditions the discriminator \mathcal{D}

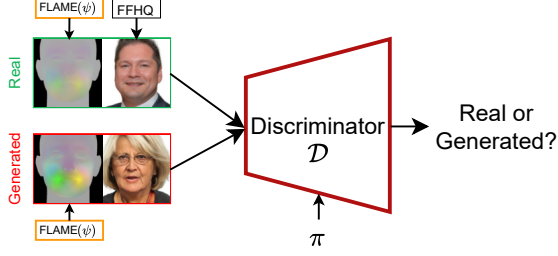


Figure 3. Dual-Discrimination. We pass synthetic renderings $S(\psi)$ along with the RGB images.

on the target expression by concatenating the rendered image with a synthetic rendering $S(\psi)$ of the FLAME mesh, where vertices are color-coded by their UV coordinates [31]. Although this improves expression consistency, the model still under-expresses high-intensity cues (see Sec. 4.4).

We therefore encode expression information more explicitly in the synthetic rendering so that the discriminator can penalize fine-grained deviations. Specifically, we color-code the posed FLAME mesh by its expression-isolated vertex displacement from the neutral pose (see Fig. 3):

$$\Delta V = V_{\text{posed}} - V_{\text{neutral}}. \quad (8)$$

Here $V_{\text{posed}} \in M(\beta_{\text{neutral}}, \psi, \theta_{\text{neutral}})$ and $V_{\text{neutral}} \in M(\beta_{\text{neutral}}, \psi_{\text{neutral}}, \theta_{\text{neutral}})$. The resulting displacement-colored rendering $S(\psi)$ is concatenated with the RGB render as input to \mathcal{D} . As we further show (see Table 3), this significantly improves expression consistency.

3.7. Loss functions & Regularizations

We train with the generator-side non-saturating GAN loss [20]:

$$\mathcal{L}_{\text{GAN}} = \text{softplus}(-\mathcal{D}(\mathcal{R}(\mathcal{A}, \pi), S(\psi), \pi)). \quad (9)$$

Following GGHEAD, we also regularize position, scale, and opacity, employing L_2 losses \mathcal{L}_{pos} , $\mathcal{L}_{\text{scale}}$ and Beta loss $\mathcal{L}_{\text{opacity}}$. In a similar fashion, we apply L_2 regularization to the position $\mathcal{L}_{\text{pos}}^D$ and scale $\mathcal{L}_{\text{scale}}^D$ residuals predicted by the deformation branch. These terms discourage large global warps and encourage the deformation branch to remain localized to fine-grained expression details.

Following prior works, we apply R1 regularization [28] on Discriminator to keep training stable.

4. Experiments

4.1. Experimental Setup

Implementation details. Our generator and discriminator models are based on StyleGAN-2 architecture. We train the model in 2 stages. First, we train it for 6.5M images using 256×256 resolution rasterization, sampling 65K gaus-

sians on UV grid. Next, we train the model for 14M images on full 512×512 resolution, sampling 262K gaussians. During both stages we use batch size 32, we set discriminator learning rate to 0.002 and generator learning rate to 0.0025. We apply R1 gradient penalty once every 16 steps with $\gamma = 1.0$ coefficient. For regularizations, we empirically choose $\lambda_{\text{pos}} = 0.25$, $\lambda_{\text{scale}} = 0.5$ for main branch and $\lambda_{\text{pos}}^D = 1.5$, $\lambda_{\text{scale}}^D = 1.5$ for deformation branch. We apply $\mathcal{L}_{\text{opacity}}$ only during the second stage and use coefficient $\lambda_{\text{opacity}} = 1.0$. The entire training takes 4 days on $4 \times \text{RTX A6000}$.

Dataset. We train our model on FFHQ [26] dataset, consisting of 75000 human head images. Following prior works, we mirror the dataset to obtain around 150000 images in total. Following GGHEAD [32], we use MODNet [29] to remove background from FFHQ images. For each image we estimate FLAME parameters via off-the-shelf estimator [46], and further derive camera parameters from estimated head rotations.

Baselines. We compare with static baselines such as GGHEAD and EG3D [6]. We also compare with state-of-the-art NeRF based animatable 3DGAN – Next3D [54] and concurrent 3DGS-based method – GAIA [68].

We employ Frechet Inception Distance (FID) to measure the quality of generated images. Following prior works [54], we use Average Pose Distance (APD), Average Expression Distance (AED) and identity consistency (ID) metrics to evaluate animation quality. To further evaluate mouth consistency, similar to GAIA we calculate the Average Jaw-pose Distance (AED-jaw). To compute metrics, we follow exactly same protocols described in [54].

We further compare inference speed of the methods on avatar reenactment setting, *i.e.* with running identity branch once with caching. To this end, we report FPS on a single RTX A6000 of PyTorch implementation of our method without any additional optimizations. For Next3D we measure FPS on the same machine using the code from the author’s repository [47]. For GAIA we take the measurements from their paper, which are also conducted on an RTX A6000 GPU with identity caching.

4.2. Comparison with SOTA

Table 1 compares AGORA with static head generators GGHEAD [32], EG3D [6] and recent animatable head avatars Next3D [54], GAIA [68]. As can be seen, our approach outperforms all other baselines in terms of image quality (FID). For camera and identity consistency, AGORA scores better in APD and ID compared to GAIA and Next3D. For the animation quality, we significantly outperform NeRF-based Next3D in both AED and AED-jaw. Compared to the concurrent work GAIA, our method produces more consistent mouth articulations, resulting in significantly better AED-jaw. While GAIA shows better ex-



Figure 4. Qualitative comparisons with Next3D on avatar generation, pose and face expression transfer.



Figure 5. Single Image avatar (PTI) comparison with Next3D.

pression consistency in AED metrics, qualitative comparison in Figure 6 demonstrates less artifacts in faces produced by our method. Finally, our method significantly outperforms previous methods in inference speed. We report 250fps and 9fps runtime on GPU and CPU (16 threads) respectively enabled by the lightweight deformation branch \mathcal{G}_d and a simple FLAME linear blend skinning of AGORA.

4.3. Qualitative Results

Avatar generation. We qualitatively compare the expressiveness of avatars generated by AGORA (ours) and Next3D. Figure 4 presents results of re-animating faces with strong expressions from the FEED dataset [16]. Our method closely follows the driving expressions and recovers fine-grained cues such as wrinkles, while remaining emotion-consistent (*i.e.* clear *disgust*, *anger*, and *surprise*). No-

Table 1. Comparison with state of the art. Lower values are better for FID/AED/APD; higher is better for ID/FPS. Best results are shown in bold. Note that EG3D and GGHEAD don’t offer expression control, so we only report FID.

Method	FID ↓	AED ↓	AED-jaw ↓	ID ↑	APD ↓	FPS ↑
EG3D [6]	3.28	—	—	—	—	—
GGHEAD [32]	4.06	—	—	—	—	—
Next3D [54]	3.18	0.930	0.046	0.74	0.031	15
GAIA [68]	3.85	0.530	<u>0.040</u>	0.72	<u>0.027</u>	<u>52</u>
Ours	3.17	<u>0.682</u>	0.021	0.75	0.025	250

tably, for the same *surprise* input our model yields age-appropriate behavior—forehead wrinkling for older subjects but not for children—enabled by shape-code conditioning, which preserves identity priors while modulating expression detail. While Next3D renders high-quality images, it often under-expresses or misaligns the target articu-

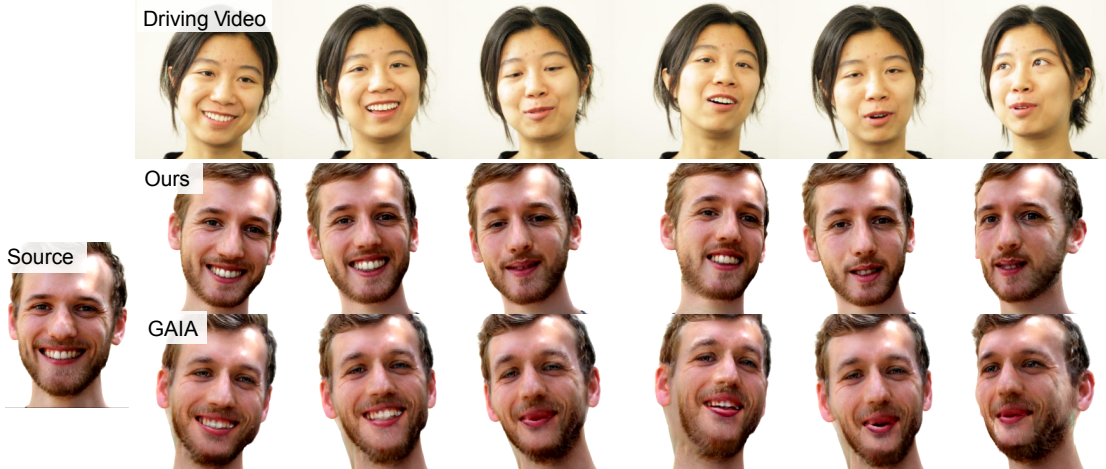


Figure 6. Single Image avatar (PTI) comparison with concurrent work GAIA.

lation in high-intensity cases.

Avatars from a single image. We further compare methods by generating avatars from a single image using Pivotal Tuning Inversion (PTI) [47]. For each source face image we run PTI to obtain its avatar, randomly assign a driving video, and transfer its expressions and camera motion. For both AGORA and Next3D we use the same PTI implementation from the authors’ repository [47]. For GAIA, we report only the PTI example provided by the authors, as their code was unavailable at the time of writing.

As illustrated in Figure 5, Next3D struggles under extreme jaw poses, exhibiting pronounced mouth/teeth artifacts, whereas AGORA maintains precise mouth articulation and better preserves identity. To perform more systematic comparison, we conduct a video-level user study using 50 in-the-wild source images (mostly public figures) and 20 driving videos, including sequences with extreme rotations and expressions from FEED [16] and additional in-the-wild talking heads. We ask people to compare AGORA and Next3D in terms of *ID consistency*, *expression consistency*, and *overall video quality* (i.e. temporal smoothness). Results of this user study in Figure 8 demonstrate consistently better performance of AGORA across all three criteria, see Section B for details.

Fig. 6 presents a qualitative comparison of our method with GAIA. We can observe frequent artifacts in mouth areas and inconsistent head geometry for GAIA-generated avatars, see e.g., column 4. In contrast, our method yields smoother motion and consistent teeth rendering. These observations can be further confirmed from video on our website¹.

Expression–identity disentanglement. In Figure 7 we assess disentanglement of expression and identity by independently interpolating the identity latent and the FLAME expression parameters. We sample two identities and two

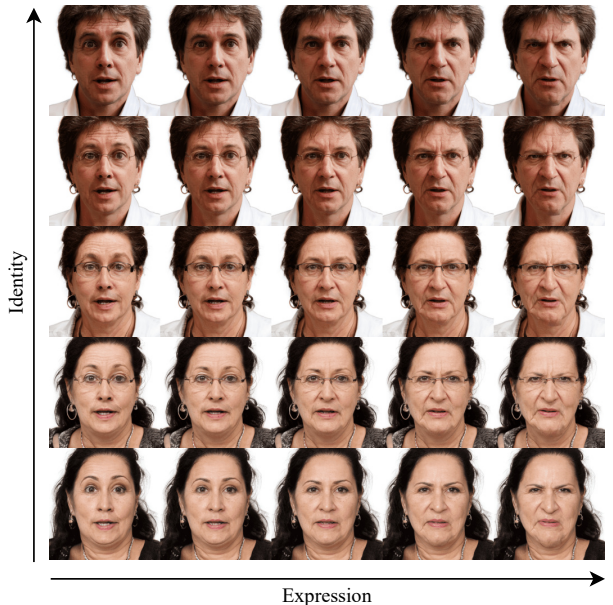


Figure 7. Expression-identity grid produced by AGORA.

expressions and obtain other identity codes and expression settings by linear interpolation. We then render the resulting grid of expressions and identities while keeping other parameters unchanged. Rows exhibit smooth expression transitions with stable identity, while columns vary identity without altering the intended expression. The grid indicates clean factor separation—precise expression changes and consistent identity traits—with no visible entanglement.

4.4. Ablation Study

We next evaluate design choices of our method. To keep ablations tractable, we report results for lightweight setting using 256×256 image resolution and 65K Gaussians. Unless stated otherwise, all variants share the same data, schedule,

¹<https://ramazan793.github.io/AGORA/>

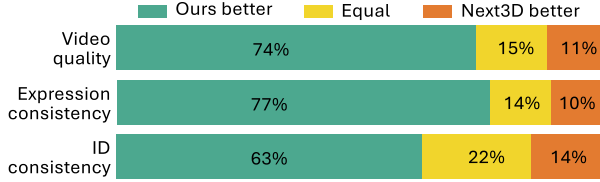


Figure 8. Results of the user study.

Table 2. Expression-Identity disentanglement. Lower is better for FID/APD/AED metrics; higher is better for ID. "S" and "D" stand for Single and Dual branch architectures.

Exp.	\mathcal{M}	\mathcal{G}	Branch	FID↓	AED↓	AED-jaw↓	ID↑	APD↓
1.	-	-	S	6.59	0.686	0.022	0.74	0.026
2.	β, ψ, θ	-	S	5.46	0.664	0.022	0.56	<u>0.027</u>
3.	-	-	D	<u>5.29</u>	0.563	<u>0.024</u>	0.56	0.026
4. (Ours)	-	β	D	4.72	<u>0.588</u>	0.022	<u>0.70</u>	0.026

and seeds under these settings.

Expression-identity disentanglement. We study the generator’s ability to faithfully represent the consistent identity, while being able to control facial expressions. To this end, we experiment with different architecture designs and present results in Table 2. The first two experiments evaluate single-branch architectures (see Figure 2(a)). We study alternative ways to condition the model with shape and expression parameters β, ψ, θ . While Exp.1 only applies linear blend skinning, Exp.2 adds β, ψ, θ to the network input. As can be seen, Exp.1 results in the worst performance with the highest values for FID and AED, indicating that additional shape and expression conditioning is essential for the model to learn appearances and facial articulations. Despite improved FID, Exp.2 results in the decreased ID consistency. This suggests that adding β, ψ, θ to the network leads to identity-expression entanglement, *i.e.* the model tends to change the identity with changed expressions.

Introduction of the deformation branch in Exp.3 results in significant improvement for both image quality (FID) and expression consistency (AED). The ID consistency of Exp.3, however, is low suggesting identity-expression entanglement. To encourage disentanglement, we use person-specific and expression-independent shape β to condition generator \mathcal{G} . The resulting model in Exp.4 demonstrates improved ID consistency while still showing excellent performance in terms of facial expressions and image quality. We conclude that the introduced identity- and expression-specific networks enable to achieve both the high generation accuracy and fast runtime, since only the lightweight expression-specific networks is executed during animation.

Discriminator Expression Conditioning. Table 3 evaluates alternative methods to condition the discriminator on expression codes. First, we show that a generator trained with a discriminator which is unaware of expressions, tends to produce incorrect expressions. In this setting the main

Table 3. Dual-Discrimination ablation. Lower is better.

Variant	AED↓	AED-jaw↓
1. w/o dual discrimination	0.832	0.024
2. cGAN-style dual discrimination	0.847	0.025
3. Next3D-style dual discrimination	0.766	0.024
4. Ours	0.588	0.022

priority for the generator is to learn high-fidelity images to trick the discriminator, which results in significantly worse AED (see row 1 in Table 3).

There are different ways to condition the discriminator on the expression code. First, we try to condition expression the same way, we condition camera parameters via cGAN-style vector projection [48]. However, we see that this doesn’t improve AED (see row 2 in Table 3). We hypothesize that camera parameters projection dominates over the expression vector, since it is easier for the discriminator to learn more obvious cues such as 3D inconsistent geometry, pose-dependent biases rather than fine-grained expression details. This results in discriminator learning to ignore expression vectors at all. For this reason we condition the generator on expression signal through image space via concatenating synthetic renderings with corresponding real/generated images. These synthetic renderings encode expression-specific geometry information and enable discriminator to implicitly learn a mapping between synthetic renderings and corresponding facial appearances. We try to learn our model with Next3D-style dual discrimination, however we observe only minor improvement of AED (see row 3 in Table 3). This occurs, because Next3D-style synthetic renderings also encode FLAME’s shapecode, which results in the discriminator memorizing the identity of the generated samples. Consequently, this pushes the generator to memorize the identity as well, so it memorizes them given pairs of shape and expression to which the model is conditioned to. Finally, this results in expression-identity entanglement. To this end, we propose to use synthetic renderings based solely on expression parameters. However, this alone is not enough, so we also generate texture for synthetic renderings in a way that colors of vertices encode LBS deformation of posed FLAME vertices. This provides to the discriminator a strong expression geometry cue and results in a major AED improvement (see row 4 (Ours) in Table 3).

5. Conclusion

We presented AGORA, a conditional 3DGS GAN for animatable head avatars. A dual-branch generator couples an identity path with an expression-specific deformation branch; spatial shape conditioning injects shape priors without collapsing diversity; and dual-discrimination on syn-

thetic geometry cues enforces precise expressions. The same model applies to single-image PTI avatars and remains stable under large poses and articulations. AGORA results in excellent generation quality, 250fps GPU runtime and interactive-rate CPU rendering while outperforming existing methods. Future work will address hair animation, adherence to variable illumination as well as extensions to full-body models.

References

- [1] Sida An, Hsiang-Chun Xu, Yichun Shi, Guoxian Song, Umit Y. Ogras, and Linjie Luo. PanoHead: Geometry-aware 3D full-head synthesis in 360deg. In *CVPR*, pages 20950–20959, 2023. 2, 13
- [2] Alexander W. Bergman, Petr Kellnhofer, Yifan Wang, Eric Chan, David B. Lindell, and Gordon Wetzstein. Generative neural articulated radiance fields. In *Adv. Neural Inform. Process. Syst.*, pages 19900–19916, 2022. 2
- [3] Shengqu Cai, Anton Obukhov, Dengxin Dai, and Luc Van Gool. Pix2nerf: Unsupervised conditional π -gan for single image to neural radiance fields translation. In *CVPR*, pages 3981–3990, 2022. 2
- [4] Ang Cao and Justin Johnson. HexPlane: A fast representation for dynamic scenes. In *CVPR*, pages 130–141, 2023. 2
- [5] Eric R. Chan, Marco Monteiro, Petr Kellnhofer, Jiajun Wu, and Gordon Wetzstein. π -gan: Periodic implicit generative adversarial networks for 3d-aware image synthesis. In *CVPR*, pages 5799–5808, 2021. 2
- [6] Eric R. Chan, Connor Z. Lin, Matthew A. Chan, Koki Nagano, Boxiao Pan, Shalini De Mello, Orazio Gallo, Leonidas J. Guibas, Jonathan Tremblay, Sameh Khamis, Tero Karras, and Gordon Wetzstein. Efficient geometry-aware 3D generative adversarial networks. In *CVPR*, pages 16123–16133, 2022. 2, 3, 5, 6
- [7] Matthew Chan, Michael Stengel, Chao Liu, Zhizun Yu, Sameh Khamis, and Koki Nagano. Real-time radiance fields for single-image portrait view synthesis. *ACM Trans. Graph.*, 2023. 3
- [8] Xu Chen, Tianjian Jiang, Jie Song, Jinlong Yang, Michael J. Black, Andreas Geiger, and Otmar Hilliges. gdna: Towards generative detailed neural avatars. In *CVPR*, 2022. 2
- [9] Yufan Chen, Lizhen Wang, Qijing Li, Hongjiang Xiao, Shengping Zhang, Hongxun Yao, and Yebin Liu. Monogaussianavatar: Monocular gaussian point-based head avatar. In *SIGGRAPH '24: ACM SIGGRAPH 2024 Conference Proceedings*. Association for Computing Machinery, 2024. 1
- [10] Xuangeng Chu and Tatsuya Harada. Generalizable and animatable gaussian head avatar. In *Adv. Neural Inform. Process. Syst.*, 2024. 3
- [11] Yu Deng, Jialong Yang, Dong Chen, Fang Wen, and Xin Tong. Disentangled and controllable face image generation via 3D imitative-contrastive learning. In *CVPR*, pages 5154–5163, 2020. 2
- [12] Yu Deng, Jialong Yang, Jianfeng Xiang, and Xin Tong. Gram: Generative radiance manifolds for 3d-aware image generation. In *CVPR*, pages 10673–10683, 2022. 2
- [13] Yudong Deng, Ding Wang, Xianfeng Ren, Xin Chen, and Baoyuan Wang. Learning one-shot 4D head avatar synthesis using synthetic data. arXiv preprint arXiv:2311.18729, 2023. 3
- [14] Yudong Deng, Ding Wang, and Baoyuan Wang. Portrait4D-v2: Pseudo multi-view data creates better 4D head synthesizer. In *Eur. Conf. Comput. Vis.*, pages 316–333. Springer, Cham, 2025. 3
- [15] Michail Christos Doukas, Soubhik Sanyal, et al. Headgan: One-shot neural head synthesis and editing. In *Int. Conf. Comput. Vis.*, 2021. 3
- [16] Nikita Drobyshev, Antoni Bigata Casademunt, Konstantinos Vougioukas, Zoe Landgraf, Stavros Petridis, and Maja Pantic. Emoportraits: Emotion-enhanced multimodal one-shot head avatars, 2024. 6, 7
- [17] Guy Gafni, Justus Thies, Michael Zollhöfer, and Matthias Nießner. Dynamic neural radiance fields for monocular 4d facial avatar reconstruction. In *Proceedings of the IEEE/CVF Conference on Computer Vision and Pattern Recognition (CVPR)*, pages 8649–8658, 2021. 1
- [18] Guy Gafni, Justus Thies, Michael Zollhofer, and Matthias Nießner. Dynamic neural radiance fields for monocular 4D facial avatar reconstruction. In *CVPR*, pages 8649–8658, 2021. 1
- [19] Simon Giebenhain, Tobias Kirschstein, Martin Rünz, Lourdes Agapito, and Matthias Nießner. NPGA: Neural parametric gaussian avatars. In *SIGGRAPH Asia 2024 Conference Papers*, pages 1–11, 2024. 1
- [20] Ian J. Goodfellow, Jean Pouget-Abadie, Mehdi Mirza, Bing Xu, David Warde-Farley, Sherjil Ozair, Aaron Courville, and Yoshua Bengio. Generative adversarial nets. In *Adv. Neural Inform. Process. Syst.*, 2014. 5
- [21] Philip-William Grassal, Malte Prinzler, Tobias Leistner, Carsten Rother, Matthias Nießner, and Justus Thies. Neural head avatars from monocular RGB videos. In *CVPR*, pages 18653–18664, 2022. 1
- [22] Jiatao Gu, Lingjie Liu, Peng Wang, and Christian Theobalt. Stylenerf: A style-based 3d-aware generator for high-resolution image synthesis. In *Int. Conf. Learn. Represent.*, 2022. 2
- [23] Xiao Han, Yuda Cao, Kai Han, Xinghui Zhu, Jian Deng, Yi-Zhe Song, and Kwang-Yee K. Wong. HeadSculpt: Crafting 3D head avatars with text. In *Adv. Neural Inform. Process. Syst.*, 2024. 2
- [24] Fangzhou Hong, Zhaoxi Chen, Yushi Lan, Liang Pan, and Ziwei Liu. Eva3d: Compositional 3d human generation from 2d image collections. In *Int. Conf. Learn. Represent.*, 2023. 2
- [25] Seung-Hwan Hyun and Jun-Pyo Heo. Adversarial generation of hierarchical gaussians for 3D generative model. arXiv preprint arXiv:2406.02968, 2024. 2
- [26] Tero Karras. A style-based generator architecture for generative adversarial networks. arXiv preprint arXiv:1812.04948, 2019. 2, 5
- [27] Tero Karras, Samuli Laine, and Timo Aila. A style-based generator architecture for generative adversarial networks. In *CVPR*, pages 4401–4410, 2019. 4

- [28] Tero Karras, Samuli Laine, Miika Aittala, Janne Hellsten, Jaakko Lehtinen, and Timo Aila. Analyzing and improving the image quality of StyleGAN. In *CVPR*, pages 8110–8119, 2020. 2, 5
- [29] Zhanghan Ke, Jiayu Sun, Kaican Li, Qiong Yan, and Rynson W.H. Lau. Modnet: Real-time trimap-free portrait matting via objective decomposition. In *AAAI*, 2022. 5
- [30] Bernhard Kerbl, Georgios Kopanas, Thomas Leimkühler, and George Drettakis. 3D gaussian splatting for real-time radiance field rendering. *ACM Trans. Graph.*, 42(4):139:1–139:12, 2023. 3
- [31] Hyeonwoo Kim, Pablo Garrido, Ayush Tewari, Weipeng Xu, Justus Thies, Matthias Niessner, Patrick Pérez, Christian Richardt, Michael Zollhöfer, and Christian Theobalt. Deep video portraits. *ACM transactions on graphics (TOG)*, 37(4): 1–14, 2018. 3, 5
- [32] Tobias Kirschstein, Simon Giebenhain, Jiapeng Tang, Michail Georgopoulos, and Matthias Nießner. GGHead: Fast and generalizable 3D gaussian heads. In *SIGGRAPH Asia 2024 Conference Papers*, pages 1–11, 2024. 2, 5, 6
- [33] Hong-geng Li, Chen Chen, Tiansong Shi, Yiren Qiu, Sida An, Guang Chen, and Xiaogang Han. SphereHead: Stable 3D full-head synthesis with spherical tri-plane representation. In *Eur. Conf. Comput. Vis.*, pages 324–341. Springer, Cham, 2025. 2
- [34] Ruilong Li, Kyle Bladin, Yipeng Zhao, Chaitanya Chinara, Owen Ingraham, Peng Xiang, and Hao Li. Learning formation of physically-based face attributes. In *CVPR*, pages 3410–3419, 2020. 2
- [35] Tianye Li, Timo Bolkart, Michael J. Black, Hao Li, and Javier Romero. Learning a model of facial shape and expression from 4D scans. *ACM Trans. Graph.*, 36(6):194:1–194:16, 2017. 2, 3
- [36] Matthew Loper, Naureen Mahmood, Javier Romero, Gerard Pons-Moll, and Michael J. Black. SMPL: A skinned multi-person linear model. In *Seminal Graphics Papers: Pushing the Boundaries, Volume 2*, pages 851–866. 2023. 2
- [37] Ben Mildenhall, Pratul P. Srinivasan, Matthew Tancik, Jonathan T. Barron, Ravi Ramamoorthi, and Ren Ng. NeRF: Representing scenes as neural radiance fields for view synthesis. *Communications of the ACM*, 65(1):99–106, 2021. 2
- [38] Thomas Müller, Alex Evans, Christoph Schied, and Alexander Keller. Instant neural graphics primitives with a multi-resolution hash encoding. *ACM Trans. Graph.*, 41(4):1–15, 2022. 2
- [39] Michael Niemeyer and Andreas Geiger. Giraffe: Representing scenes as compositional generative neural feature fields. In *Adv. Neural Inform. Process. Syst.*, 2020. 2
- [40] Maxime Oquab, Timothée Darcet, Julien Mairal, and Philipp Bojanowski. Dinov2: Learning robust visual features without supervision. *arXiv preprint arXiv:2304.07193*, 2023. 3
- [41] Roy Or-El, Xuan Luo, Mengyi Shan, Eli Shechtman, Jeong Joon Park, and Ira Kemelmacher-Shlizerman. Stylesdf: High-resolution 3d-consistent image and geometry generation. In *CVPR*, 2022. 2
- [42] Xingang Pan, Xudong Xu, Chen Change Loy, Christian Theobalt, and Bo Dai. A shading-guided generative implicit model for shape-accurate 3d-aware image synthesis. In *Adv. Neural Inform. Process. Syst.*, 2021. 2
- [43] Pascal Paysan, Reinhard Knothe, Brian Amberg, Sami Romdhani, and Thomas Vetter. A 3D face model for pose and illumination invariant face recognition. In *2009 Sixth IEEE International Conference on Advanced Video and Signal Based Surveillance*, pages 296–301. IEEE, 2009. 2
- [44] Ben Poole, Ajay Jain, Jonathan T. Barron, and Ben Mildenhall. DreamFusion: Text-to-3D using 2D diffusion. *arXiv preprint arXiv:2209.14988*, 2022. 2
- [45] Shenhan Qian, Tobias Kirschstein, Lukas Schoneveld, Davide Davoli, Simon Giebenhain, and Matthias Nießner. GaussianAvatars: Photorealistic head avatars with rigged 3D gaussians. In *CVPR*, pages 20299–20309, 2024. 1
- [46] George Retsinas, Panagiotis P. Filntisis, Radek Danecek, Victoria F. Abrevaya, Anastasios Roussos, Timo Bolkart, and Petros Maragos. 3d facial expressions through analysis-by-neural-synthesis. In *CVPR*, 2024. 5
- [47] Daniel Roich, Ron Mokady, Amit H. Bermanto, and Daniel Cohen-Or. Pivotal tuning for latent-based editing of real images. *ACM Trans. Graph.*, 42(1):1–13, 2022. 5, 7
- [48] Axel Sauer, Kashyap Chitta, Jens Müller, and Andreas Geiger. Projected gans converge faster. In *Advances in Neural Information Processing Systems (NeurIPS)*, 2021. 8
- [49] Katja Schwarz, Yiyi Liao, Michael Niemeyer, and Andreas Geiger. Graf: Generative radiance fields for 3d-aware image synthesis. In *Adv. Neural Inform. Process. Syst.*, 2020. 2
- [50] Katja Schwarz, Axel Sauer, Michael Niemeyer, Yiyi Liao, and Andreas Geiger. Voxgraf: Fast 3d-aware image synthesis with sparse voxel grids. In *Adv. Neural Inform. Process. Syst.*, 2022. 2
- [51] Ivan Skorokhodov, Sergey Tulyakov, Yiqun Wang, and Peter Wonka. Epigraf: Rethinking training of 3d gans. In *Adv. Neural Inform. Process. Syst.*, 2022. 2
- [52] Jingxiang Sun, Xuan Wang, Yichun Shi, Lizhen Wang, Jue Wang, and Yebin Liu. Ide-3d: Interactive disentangled editing for high-resolution 3d-aware portrait synthesis. *ACM Trans. Graph.*, 2022. 2
- [53] Jingxiang Sun, Xuan Wang, Yong Zhang, Xiaoyu Li, Qi Zhang, Yebin Liu, and Jue Wang. Fenerf: Face editing in neural radiance fields. In *CVPR*, 2022. 2
- [54] Jing Sun, Xuan Wang, Lizhen Wang, Xiaoyu Li, Yebin Zhang, Hao Zhang, and Yan-Pei Liu. Next3D: Generative neural texture rasterization for 3D-aware head avatars. In *CVPR*, pages 20991–21002, 2023. 2, 4, 5, 6, 12
- [55] Jiapeng Tang, Davide Davoli, Tobias Kirschstein, Lukas Schoneveld, and Matthias Niessner. GAF: Gaussian avatar reconstruction from monocular videos via multi-view diffusion. *arXiv preprint arXiv:2412.10209*, 2024. 2
- [56] Justus Thies, Michael Zollhöfer, Marc Stamminger, Christian Theobalt, and Matthias Nießner. Face2face: Real-time face capture and reenactment of rgb videos. In *Proceedings of the IEEE Conference on Computer Vision and Pattern Recognition (CVPR)*, 2016. 3
- [57] Phong Tran, Egor Zakharov, Long-Nhat Ho, Liwen Hu, Aleksei Karmanov, Aayush Agarwal, and Hao Li. VODOO XP: Expressive one-shot head reenactment for VR telepresence. *arXiv preprint arXiv:2405.16204*, 2024. 3

- [58] Phong Tran, Egor Zakharov, Long-Nhat Ho, Anh-Tuan Tran, Liwen Hu, and Hao Li. VOODOO 3D: Volumetric portrait disentanglement for one-shot 3D head reenactment. In *CVPR*, pages 10336–10348, 2024. [3](#)
- [59] Alex Trevithick, Matthew Chan, Towaki Takikawa, Umar Iqbal, Shalini De Mello, Manmohan Chandraker, Ravi Ramamoorthi, and Koki Nagano. What you see is what you GAN: Rendering every pixel for high-fidelity geometry in 3d GANs. In *CVPR*, 2024. [2](#)
- [60] Xintao Wang, Yu Li, Honglun Zhang, and Ying Shan. Towards real-world blind face restoration with generative facial prior. In *CVPR*, pages 9168–9178, 2021. [2](#)
- [61] Yating Wang, Xuan Wang, Ran Yi, Yanbo Fan, Jichen Hu, Jingcheng Zhu, and Lizhuang Ma. 3d gaussian head avatars with expressive dynamic appearances by compact tensorial representations. In *Proceedings of the IEEE/CVF Conference on Computer Vision and Pattern Recognition (CVPR)*, pages 21117–21126, 2025. [1](#)
- [62] Yue Wu, Yu Deng, Jiaolong Yang, Fangyun Wei, Qifeng Chen, and Xin Tong. Anifacegan: Animatable 3d-aware face image generation for video avatars. In *Adv. Neural Inform. Process. Syst.*, 2022. [2](#)
- [63] Lin Xie, Xuan Wang, Hang Zhang, Chao Dong, and Ying Shan. VFHQ: A high-quality dataset and benchmark for video face super-resolution. In *CVPR*, pages 657–666, 2022. [2](#), [3](#)
- [64] Hsiang-Chun Xu, Guoxian Song, Zihang Jiang, Jianfeng Zhang, Yichun Shi, Jiaming Liu, and Linjie Luo. OmniAvatar: Geometry-guided controllable 3D head synthesis. In *CVPR*, pages 12814–12824, 2023. [2](#)
- [65] Yinghao Xu, Sida Peng, Ceyuan Yang, Yujun Shen, and Bolei Zhou. 3d-aware image synthesis via learning structural and textural representations. In *CVPR*, 2022. [2](#)
- [66] Yuelang Xu, Bo Chen, Zhaoyang Li, Hong Zhang, Ligang Wang, Zhiyong Zheng, and Yan-Pei Liu. Gaussian head avatar: Ultra high-fidelity head avatar via dynamic gaussians. In *CVPR*, pages 1931–1941, 2024. [1](#)
- [67] Wang Yu, Yan-Pei Fan, Yichao Zhang, Xiao-Ming Wang, Fei Yin, Yang Bai, and Bo Wu. NOFA: NeRF-based one-shot facial avatar reconstruction. In *ACM SIGGRAPH 2023 Conference Proceedings*, pages 1–12, 2023. [3](#)
- [68] Zhengming Yu, Tianye Li, Jingxiang Sun, Omer Shapira, Seonwook Park, Michael Stengel, Matthew Chan, Xin Li, Wenping Wang, Koki Nagano, et al. Gaia: Generative animatable interactive avatars with expression-conditioned gaussians. In *Proceedings of the Special Interest Group on Computer Graphics and Interactive Techniques Conference Conference Papers*, pages 1–10, 2025. [2](#), [3](#), [5](#), [6](#)
- [69] Egor Zakharov, Aliaksandr Shysheya, Egor Burkov, and Victor Lempitsky. Few-shot adversarial learning of realistic neural talking head models. *arXiv preprint arXiv:1905.08233*, 2019. [3](#)
- [70] Yufeng Zheng, Victoria Fernández Abrevaya, Marcel C. Bühler, Xu Chen, Michael J. Black, and Otmar Hilliges. I M Avatar: Implicit morphable head avatars from videos. In *Proceedings of the IEEE/CVF Conference on Computer Vision and Pattern Recognition (CVPR)*, pages 13545–13555, 2022. [1](#)
- [71] Yufeng Zheng, Yifan Wang, Gordon Wetzstein, Michael J. Black, and Otmar Hilliges. PointAvatar: Deformable point-based head avatars from videos. In *CVPR*, pages 21057–21067, 2023. [1](#)
- [72] Peng Zhou, Lingxi Xie, Bingbing Ni, and Qi Tian. Cips-3d: A 3d-aware generator of gans based on conditionally-independent pixel synthesis. *arXiv preprint arXiv:2110.09788*, 2021. [2](#)
- [73] Zhen Zhou, Feitong Ma, Hsin-Ying Fan, and Yilin Yang. HeadStudio: Text to animatable head avatars with 3D gaussian splatting. *arXiv preprint arXiv:2402.06149*, 2024. [2](#)
- [74] Wojciech Zielonka, Timo Bolkart, and Justus Thies. Instant volumetric head avatars. In *CVPR*, pages 4574–4584, 2023. [1](#)

AGORA: Adversarial Generation Of Real-time Animatable 3D Gaussian Head Avatars

Appendix

We provide additional implementation details and experimental protocols to support the main paper. We begin by describing the topological modifications to the FLAME template (Sec. A). We then outline our experimental evaluation, including the user study configuration (Sec. B) and quantitative metric protocols (Sec. C). Next, we provide architectural details for the deformation branch (Sec. D), compare our dual-discrimination with Next3D (Sec. E), and describe the spatial shape conditioning (Sec. F). Finally, we report hardware specifications (Sec. G), followed by a discussion on limitations (Sec. H) and ethical considerations (Sec. I).

A. FLAME template with mouth

We use a slightly modified FLAME2020 template. In particular, we extend it with mouth interior by adding a mouth cavity and two (upper/lower) rows of frontal teeth. For the mouth cavity, we derive skinning weights by averaging the upper- and lower-lip weights and mixing them 50/50 as vertices approach the deepest point of the cavity. For shape and expression blendshapes, we reuse those of the upper/lower lips. For pose blendshapes, we take the upper/lower-lip correctives and blend them 50/50 toward the cavity apex. Since our training data lacks back-head supervision, we remove the back-head region and fill the resulting UV hole by stretching neighboring side regions.

B. User study details

We run a video-level, three-question forced-choice study with an optional `equal` (tie) option. Each participant answers three questions per video: ID consistency, expression consistency, and overall video quality. Each participant rates 25 of the 50 video pairs; participants are split into two groups to cover all pairs. In the interface, we first show a static *target* portrait (identity to match). Below it, each trial presents a three-panel comparison video: *LEFT* = Method A, *MIDDLE* = real driving video, *RIGHT* = Method B. We randomly swap the left/right assignment of methods on every trial. In the UI, `method_1` corresponds to ours and `method_2` to Next3D.

We discard `equal` votes and evaluate significance with a two-sided binomial test against 50% on decisive votes. Table 4 summarizes the results.

Table 4. Pairwise preference (ours vs. Next3D) on decisive votes. We report two-sided binomial p -values.

	method_1 (ours)	method_2 (Next3D)	Ties (abs)	Win rate (ours, %)	p -value (binomial)
q1 (ID)	335	76	117	81.5	$< 10^{-39}$
q2 (Expression)	405	51	72	88.8	$< 10^{-68}$
q3 (Quality)	389	58	81	87.0	$< 10^{-60}$

C. Metric computation

We follow the evaluation protocol of Next3D [54]. FID is computed on FFHQ using 50k random samples drawn from the latent, camera, and FLAME parameter distributions; for 256² baselines we use FFHQ-256. For AED and APD, we randomly sample 500 identities and, for each, 20 random {expression, pose} pairs. We re-estimate FLAME parameters from generated images and compute the mean distance to the driving parameters. The ID score is calculated as the mean ArcFace cosine similarity between 1000 generated image pairs of the same identity under different poses and expressions. Cropping and alignment are consistent with training.

D. Deformation branch architecture details

We deliberately design the expression-specific branch to be lightweight. It takes as input 64×64 features from the main branch, which encode identity-related structure, and predicts 256×256 expression-specific UV-space deformations of the Gaussian attributes via two consecutive StyleGAN2 blocks (see Figure 9). The deformation branch has only ~ 3 M parameters, compared to ~ 30 M for the identity branch, enabling real-time avatar animation at inference.

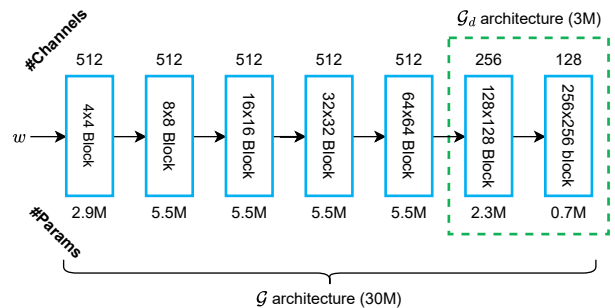


Figure 9. Architecture of identity- and expression-specific branches (StyleGAN2 blocks).

E. Comparison to Next3D’s dual discrimination

We visually compare our dual-discrimination synthetic renderings with those from the Next3D approach (Figure 10). We observe that our renderings provide stronger expression-specific cues, enabling the discriminator to more effectively penalize the generator for expression inaccuracies.

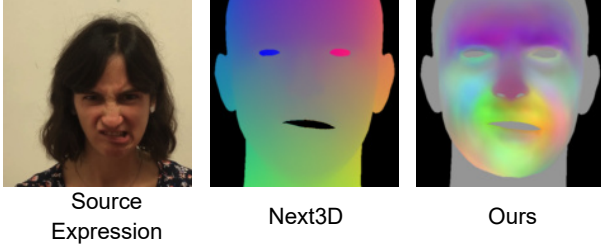


Figure 10. Comparison of synthetic renderings $S(\psi)$.

F. Spatial shape conditioning details

Given the FLAME shape code, we generate a UV-aligned field of shape-induced XYZ residuals (see Figure 11) and inject these features into every StyleGAN block of the main generator.

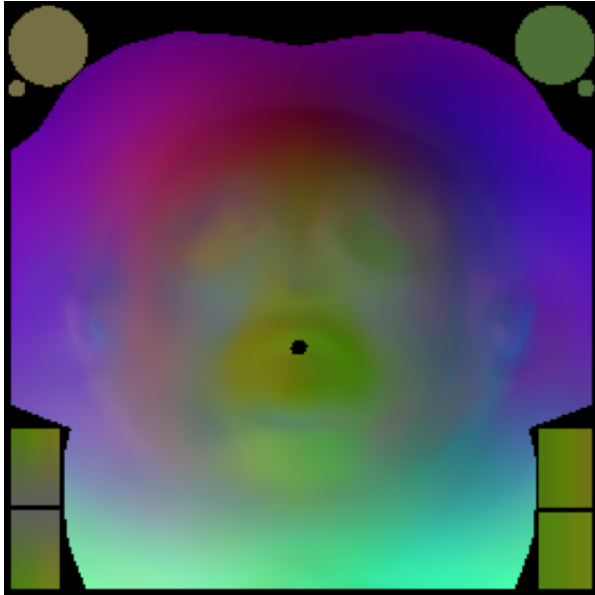


Figure 11. Each pixel encodes the vertex XYZ displacement w.r.t. the template.

G. Hardware details

For CPU inference measurements, we use an Intel Xeon Platinum 8570 CPU and run naive PyTorch CPU infer-

ence with 16 threads. For GPU inference, we use a single NVIDIA RTX A6000.

H. Limitations

Our current model is trained and evaluated on frontal heads and does not synthesize the back of the head. This limitation can be alleviated by supervising with 360° full-head data, in the spirit of PanoHead [1]. In addition, we do not control ocular gaze: the generator is not conditioned on gaze and the FLAME parameters we estimate exclude eyeball rotations. A practical path forward is to obtain per-image gaze from state-of-the-art monocular gaze estimators during training and map these predictions to FLAME’s eyeball joints, enabling explicit gaze control at inference. Beyond gaze and back-of-head synthesis, we also leave hair animation and illumination handling to future work

I. Ethical considerations

AGORA produces identity-preserving, controllable head avatars at real-time rates, even on CPU – which lowers the barrier to large-scale deployment and introduces dual-use risks (*e.g.*, unauthorized identity cloning, consentless personalization, and misuse in telepresence or misinformation). In our experiments we rely on publicly available datasets and do not train on private images; for any release we will provide usage guidelines that require proof of consent for single-image personalization. We explicitly discourage use for impersonation and encourage research on consent-aware editing and robust content provenance to complement technical advances.